CellPress

Chemistry & Biology
Article

Identification of Orai1 Channel Inhibitors by Using Minimal Functional Domains to Screen Small Molecule Microarrays

Amir Masoud Sadaghiani,[1,2,8] Sang Min Lee,[3] Justin I. Odegaard,[4] Dennis B. Leveson-Gower,[5] Olivia M. McPherson,[6] Paul Novick,[7] Mi Ri Kim,[3] Angela N. Koehler,[6] Robert Negrin,[5] Ricardo E. Dolmetsch,[2,8,*] and Chan Young Park[2,3,*]
[1]Department of Chemical and Systems Biology, Stanford University School of Medicine, Stanford, CA 94305, USA
[2]Department of Neurobiology, Stanford University School of Medicine, Stanford, CA 94305, USA
[3]Department of Biological Sciences, Ulsan National Institute of Science and Technology (UNIST), 689-798 Ulsan, South Korea
[4]Department of Pathology, Stanford University School of Medicine, Stanford, CA 94305, USA
[5]Department of Medicine, Stanford University School of Medicine, Stanford, CA 94305, USA
[6]Broad Institute of MIT and Harvard, Cambridge, MA 02139, USA
[7]Department of Chemistry, Stanford University School of Medicine, Stanford, CA 94305, USA
[8]Novartis Institutes for Biomedical Research, Cambridge, MA 02139, USA
*Correspondence: ricardo.dolmetsch@novartis.com (R.E.D.), cypark@unist.ac.kr (C.Y.P.)
http://dx.doi.org/10.1016/j.chembiol.2014.08.016

SUMMARY

Store-operated calcium (SOC) channels are vital for activation of the immune cells, and mutations in the channel result in severe combined immunodeficiency in human patients. In lymphocytes, SOC entry is mediated by the Orai1 channel, which is activated by direct binding of STIM1. Here we describe an alternative approach for identifying inhibitors of SOC entry using minimal functional domains of STIM1 and Orai1 to screen a small-molecule microarray. This screen identified AnCoA4, which inhibits SOC entry at submicromolar concentrations and blocks T cell activation in vitro and in vivo. Biophysical studies revealed that AnCoA4 binds to the C terminus of Orai1, directly inhibiting calcium influx through the channel and also reducing binding of STIM1. AnCoA4, unlike other reported SOC inhibitors, is a molecule with a known binding site and mechanism of action. These studies also provide proof of principle for an approach to ion channel drug discovery.

INTRODUCTION

Calcium is the most abundant second messenger in cell signaling, and its tight regulation is necessary for a broad variety of cellular events, including proliferation, migration, and gene expression. Store-operated calcium (SOC) channels are the major source of calcium influx in many nonexcitable cells, including T lymphocytes and mast cells. SOC entry is activated by inositol-phosphate-coupled production of phosphatidylinositol 4, 5 bisphosphate (inositol 1,4,5-trisphosphate [IP3]), which binds to IP3 receptors in the endoplasmic reticulum (ER) and causes release of calcium from ER calcium stores. Depletion of ER calcium stores triggers calcium influx across the cell membrane, which is essential for activating biochemical cascades in immune cells and leads to changes in gene expression, cytokine production, and cell proliferation.

SOC entry is mediated by calcium-release-activated calcium (CRAC) channels, which are composed of the proteins STIM and Orai (Hoth and Penner, 1992; Lewis and Cahalan, 1989). STIM1 and its close homolog STIM2 are single-transmembrane-domain proteins that reside mainly in the membrane of the ER and form the ER calcium sensor of the channel. Orai1 1, 2, and 3 are transmembrane-domain proteins that are localized in the plasma membrane and form the pore of the channel (Feske et al., 2006; Liou et al., 2005; Roos et al., 2005; Vig et al., 2006). Depletion of calcium from the ER leads to a conformational change in an EF-hand calcium-binding domain of STIM, causing STIM aggregation into puncta and exposing an Orai1-binding domain called the CRAC-activating domain (CAD) (Park et al., 2009). CAD binds to Orai1, clustering Orai1 into puncta and opening the channel, thus leading to calcium influx into the cell from the extracellular environment.

Although STIM and Orai are expressed in a variety of tissues, they are particularly important in the function of immune cells. Orai1 and STIM1 are the major source of calcium entry in human immune cells and are required for immune cell activation (Gwack et al., 2007; McCarl et al., 2010; Oh-Hora et al., 2008). Homozygous mutations in human Orai1 and STIM1 cause severe combined immunodeficiency (SCID) syndrome in human patients (Feske et al., 2006; McCarl et al., 2009). Loss of function of Orai1 and STIM1 in mouse models causes defects in Th1, Th2, Th17, B cell, and platelet activation (Feske, 2007; Feske, 2010; Shaw and Feske, 2012).

Because of their central importance in regulation of the immune system, the SOC channels have been the target of several drug discovery efforts. The main intracellular target of calcium influx through SOC channels is the calcium-regulated phosphatase calcineurin. Calcineurin dephosphorylates the nuclear factor of activated T cells (NFAT) family of transcription factors that regulate pathways of gene expression required for the production of cytokines, such as IL2, IL3, and TNFα, that affect

immune response (Hogan et al., 2010). Calcineurin is an important clinical target for immune modulation, and calcineurin inhibitors cyclosporin A (CsA) and tacrolimus are the most widely used immunosuppressant agents in patients.

Clinically approved immunosuppressant agents such as CsA and steroids have a number of potentially serious side effects, including hypertension, nephrotoxicity, and liver damage (Burdmann et al., 2003; Hoorn et al., 2011). It has been proposed that inhibitors of Orai1 might have fewer side effects, as Orai1 channels play a much more specific and well-defined role in SOC influx than cyclophilin and FKBP12, which are the targets of CsA and tacrolimus. This hypothesis is supported by the observation that patients with Orai1 mutations have SCID, mild muscular myotonia, and ectodermal dysplasia but are largely free of other disorders (Feske, 2009; Shaw and Feske, 2012). Several groups have therefore begun to look for blockers of Orai1 channels, and relatively nonspecific blockers have been described, including 2APB, a repurposed inositol trisphosphate receptors inhibitor, and YM-58483 (Diver et al., 2001; Takezawa et al., 2006). A recent paper from a group at Hoffmann-La Roche reported the discovery of RO2959, a relatively potent CRAC channel inhibitor with half maximal inhibitory concentration (IC_{50}) values of about 200 nM, depending on the assay (Chen et al., 2013). To achieve these IC_{50} values, however, this molecule had to be preincubated with cells for 30 to 60 min, suggesting that it may act on Orai1 indirectly. This compound and most of the other Orai1 inhibitors that have been published were identified using cell-based screening assays. One disadvantage of this approach is that the molecular mechanism by which it blocks Orai1 is not understood. Specifically, it is not known whether this compound binds directly to Orai1 or inhibits the channel by binding to a different protein. This lack of understanding of the binding site and mechanism makes it difficult to improve the specificity or pharmacodynamics of the compound using structure function studies.

Here, we report an alternative approach for identifying inhibitors of CRAC channel function that takes advantage of existing knowledge of the minimal functional domains (MFD) of ion channel proteins. We generated in vitro purified peptides encompassing Orai1 and STIM1 domains that are important for the gating of the SOC ion channels. Using these domains, we rapidly and inexpensively screened a small-molecule microarray (SMM) and identified several blockers of Orai1. We characterized the mechanism and showed that one of these blockers, AnCoA4, binds to and inhibit the Orai1 channel. We then demonstrated that AnCoA4 is an effective immunosuppressant in vitro and in vivo. This platform could dramatically increase the speed of screening efforts and efficiency of lead compound optimization for various ion channels.

RESULTS

SMM Screen for Inhibitors of SOC

Since the discovery of STIM1 and Orai1, important functional domains of these proteins have been identified by various groups. The N terminus of Orai1 binds directly to STIM1, calmodulin, and SPCA2 and plays an important role in channel gating and inactivation (Feng et al., 2010; Mullins et al., 2009; Park et al., 2009). The C terminus of Orai1 also binds to STIM1 and is essential for gating of the channel as well for aggregation into clusters at ER-plasma membrane junctions (Frischauf et al., 2009; Muik et al., 2008). Structure function analysis of STIM proteins has also revealed several important functional domains, including the EF-hand and SAM domains in the lumen that are important for calcium store-dependent conformational changes and the CAD, a 107 amino acid fragment of the STIM1 molecule that by itself can activate Orai1 channels by directly binding to its N and C termini (Park et al., 2009). Discovery of these MFDs of STIM1 and Orai1 and understanding their mechanism of action provides an opportunity to identify small molecules that bind to these domains and can modify different aspects of channel function.

SMMs are collections of organic molecules arrayed on modified glass slides (Seiler et al., 2008; Vegas et al., 2008). They provide a fast and inexpensive method for identifying small molecules that bind to specific proteins and have been used to obtain inhibitors of tyrosinases, γ-secretase, and cathepsins, among others (Shi et al., 2009, 2011). To identify small molecules that bind to the MFDs of Orai1 and STIM1, we generated glutathione S-transferase (GST) fusions of the CAD of STIM1 and MFDs in the N terminus, 2-3 loop, and C terminus of Orai1 (Figures S1A and S1B available online). We then incubated SMMs containing 12,000 compounds with the GST fusion proteins, and fluorescent anti-GST antibodies were used to detect binding of the MFDs to specific compounds immobilized on the SMMs (Figure 1A). The screen was carried out in triplicate, and a composite *Z* score was calculated for the binding of each small molecule (Figure 1B). Although the outcome of this screen using the GST-CAD was not robust enough, resulting in compounds with low composite *Z* scores, we identified 120 compounds that bound to the Orai1 peptides with composite *Z* score values of three SDs from the mean (Figure 1C; Figures S1C and S1D). Fifty-one of these were commercially available and were prioritized for evaluation in secondary functional assays.

To determine whether these compounds affected the function of Orai1 and STIM1 in intact cells, we used a NFAT reporter gene assay in human embryonic kidney 293T (HEK293T) cells. Activation of STIM1 and Orai1 results in calcium influx and subsequent dephosphorylation and activation of the NFAT transcription factor. We first treated cells with each of the 51 compounds at a single dose (50 μM) for 6 hr in the presence of 1 μM thapsigargin (TG) to activate SOC entry and measured NFAT-luciferase expression (Figure 1D). We used *Renilla* luciferase as an internal control to monitor the viability of cells (Figure 1E). To confirm that AnCoA4 does not cause gross toxicity, we tested cell viability in rat basophilic leukemia (RBL) cells using a 1-N-methyl-5-thiotetrazole (MTT) assay (Figure S1E). Four of the 51 compounds suppressed the activation of the NFAT-luciferase reporter gene without affecting cell viability, suggesting that they inhibit Orai1 channel activation. We next generated dose-response curves for these four compounds and found that AnCoA5 (compound 25) and AnCoG4 (compound 23) inhibited NFAT-luciferase only at concentrations greater than 10 μM (Figures 1F and 1G). In contrast, AnCoF6 (compound 38) and AnCoA4 (compound 17), which differ by only a methoxy group, inhibited NFAT-luciferase with much higher potency (Figures 1H and 1I). AnCoA4 showed the highest potency with an half maximal effective concentration (EC_{50}) value of 880 nM (Figure 1J).

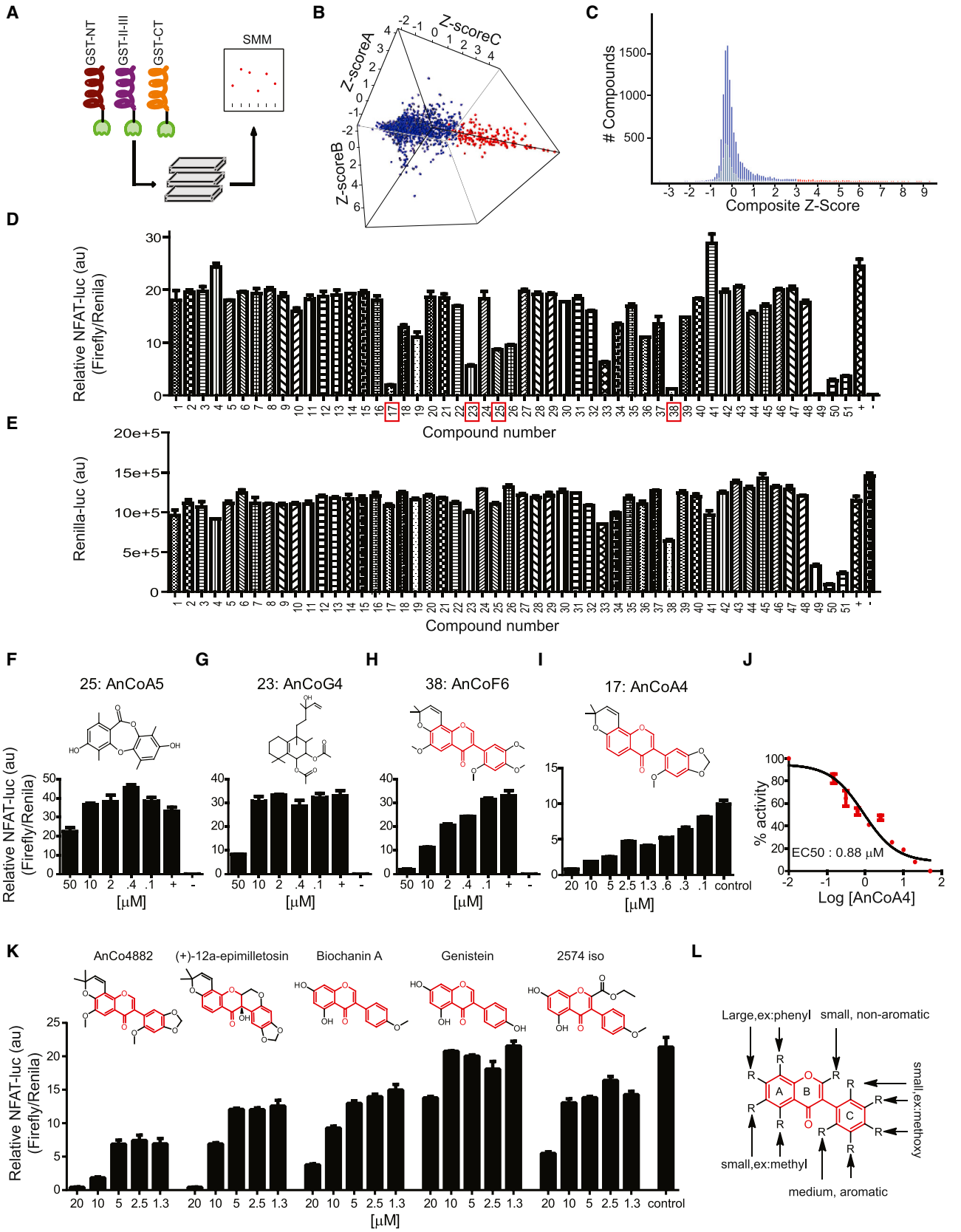

(legend on next page)

We next investigated the structure-activity relationship (SAR) of AnCoA4 by treating cells with compounds related to AnCoA4 and measuring NFAT luciferase expression. AnCo4882, which also differs from AnCoA4 only by a methoxy group, showed almost complete inhibition at 20 μM. 12a-Epimilletosin, which has a more sterically hindered structure and a hydroxyl replacement of the double bond on carbon 3, also demonstrated strong inhibition at 20 μM. Biochanin A showed a weaker dose-dependent inhibition, while removing all the methoxy groups to generate genistein abolished all activity. Methylation and addition of an ethyl ester in 2574 ISO restored some of the activity to genistein (Figure 1K). On the basis of these findings, we determined that the core structure required for activity is composed of an isoflavone-like structure containing three rings. The aromatic ring C tolerates small methoxy substituents, while the aromatic ring A can accept a phenyl ring (Figure 1L). Addition of large groups on ring B seemed to reduce activity of the analogs. This suggests that the best site for modifying this class of molecules to generate additional Orai1 inhibitors would be on the aromatic ring A. We have since made several synthetic analogs to enhance the potency and drug-likeness of this class of inhibitors (Figure S2). AnCoA4 remained the best inhibitor for our studies, as most of the analogs were less potent or had lost their ability to inhibit SOC at all.

AnCoA4 Inhibits SOC-Induced Calcium Influx

To further confirm the validity of our binding screen, we next investigated whether AnCoA4 inhibits NFAT activity by inhibiting the calcium influx pathway of SOC. We first tested whether AnCoA4 acts through inhibition of calcineurin, a phosphatase that is activated by binding to calcium upon activation of SOC. Calcineurin is responsible for dephosphorylation of NFAT and its translocation to the nucleus. Ectopic expression of a constitutively active calcineurin blocked the ability of AnCoA4 to inhibit the luciferase signal, suggesting that AnCoA4 acts upstream of calcineurin (Figure S3). Because calcium is the direct activator of calcineurin and it permeates the cell membrane through Orai1, we measured SOC-specific calcium influx using Fura-2 to measure SOC elevations in HEK293T cells in the presence (50 μM) or absence of compounds identified from the secondary screen. AnCoA4 nearly abolished SOC-dependent intracellular calcium influx compared with DMSO-treated control (Figures 2A and 2B), while AnCoF6 caused a significant reduction in the calcium rise (Figure 2C). In agreement with the results from the luciferase screen, AnCoA5 and AnCoG4, which have very different chemical structures from AnCoA4, were not as effective at inhibiting SOC (Figures 2D and 2E). The analogs of AnCoA4 also inhibited calcium influx, with AnCo4882 having the most potent effect (Figures 2F and 2G), followed by 12a-epimilletosin (Figure 2H) and biochanin A (Figure 2I). To exclude the possibility that these compounds inhibit SOC by preventing the depletion of calcium stores, we measured the release of calcium from the ER directly. We saw no evidence of the compounds' inhibiting the release of calcium from the ER in the absence of extracellular calcium (Figure 2J).

AnCoA4, AnCoF6, and AnCoA5 also caused a significant decrease in the influx slope of the intracellular calcium elevation, providing additional evidence that they inhibit calcium influx rather than release of calcium from stores. Surprisingly, AnCoG4 caused a modest increase in the slope of the calcium rise, suggesting that it increases calcium flux through the channel (Figure 2K). Finally, all of the analogs of AnCoA4 caused a significant decrease in the slope of influx (Figure 2L). Together, these results suggest that the compounds identified by the MFD screen inhibit SOC influx in cells. To gain some insight about the specificity of these compounds for SOC, we also tested the effect of these compounds on voltage-gated calcium channels in SH-SY5Y cells. Although we recognize that enhancement of potency and specificity is a challenging task that comes after hit identification in a screen, it was encouraging to observe that AnCoA4 (10 μM) had no effect on voltage-gated calcium channels, supporting the idea that AnCoA4 is relatively specific for SOC (Figure S4).

To provide direct evidence that AnCoA4 inhibits Orai1 channels, we performed whole-cell patch-clamp recordings in a HEK293 cell line stably coexpressing STIM1 and Orai1. After depletion of calcium stores, cells maintained a relatively constant level of CRAC current (I_{CRAC}) over 1,000 s. Acute application of 20 μM AnCoA4 resulted in an 80% decrease in calcium currents (Figures 3A–3C). The inhibition was dose dependent but was only partially reversed by removing the compound, pointing to a slow effective off rate of AnCoA4 from the channel. AnCoA4 did not alter the current-voltage relationship of I_{CRAC}, indicating that it does not change the channel's ion selectivity (Figure 3D).

Figure 1. SMM Screen and Validation of Potential Inhibitors of SOC by NFAT-Luciferase

(A) Schematic of SMM screen. Purified GST-fused MFDs were incubated with SMMs, and binding of MFDs to surface-immobilized small molecules was detected using fluorescent-tagged anti-GST antibody.

(B) Scatterplot of normalized *Z* scores for the binding of the small molecules to MFDs. Each axis represents an independent SMM replicate treated with a pool of GST-fused Orai1 MFDs. Gray dots represent background binding. Blue dots are true test compounds with low binding, and red dots represent chemical compounds that bound to MFDs with high affinity on the basis of their *Z* scores.

(C) Histogram of replicate-averaged *Z* scores of hit compounds with background correction. Blue bars show low affinity and nonspecific small-molecule binders. Red bars represent consistent tight binding molecules to MFDs that were picked as potential hits for follow-up studies.

(D) Fifty-one selected compounds were tested for inhibition of SOC-dependent NFAT-luciferase activity in HEK293T cells. Compounds exhibiting significant NFAT-luciferase inhibition with normal cell viability are highlighted in red rectangles. Each number represents a compound, (+) represents DMSO treatment alone, and (-) represents no addition of TG and PMA for activation of NFAT-luciferase. All measurements were taken 6 hr after the addition of TG and PMA. All error bars represent SEM.

(E) Viability measurements using *Renilla* luciferase activity driven by SOC-independent promoter.

(F–I) Dose-response measurements of NFAT-luciferase activity shows mild inhibition for AnCoA5 (F), inhibition at highest concentration for AnCoG4 (G), a well-correlated dose-response for AnCoF6 (H), and AnCoA4 (I).

(J) Dose-response curve of AnCoA4 calculated from (I). The calculated EC_{50} is 0.88 μM.

(K) Analogs of AnCoA4: AnCo4882 (+)-12a-epimilletosin, biochanin A, genistein, 2574 ISO were tested using NFAT-luciferase assay to determine SAR.

(L) Core active structure (red) and predicted suitable constituents determined from SAR studies.

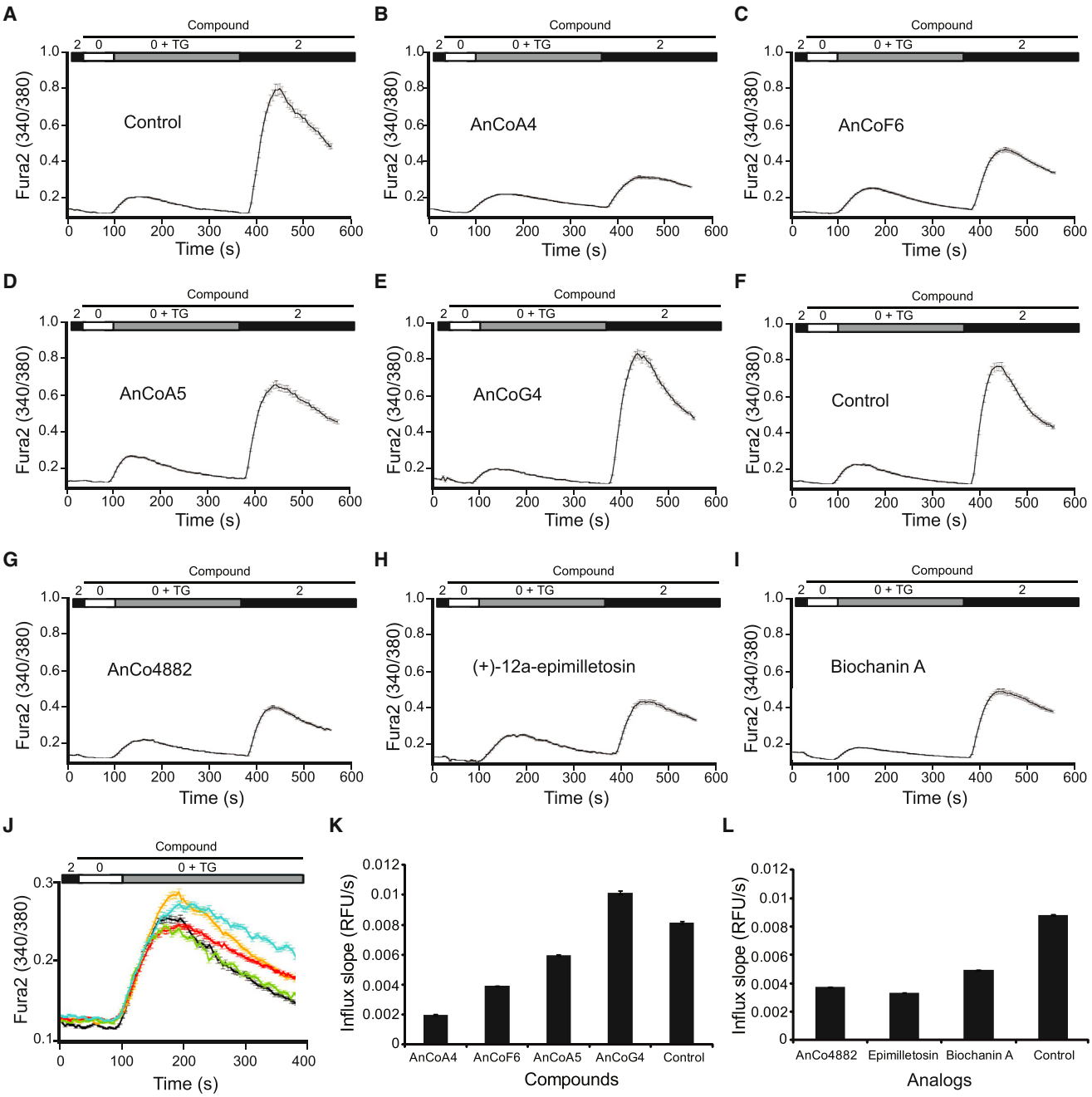

Figure 2. AnCoA4 and Its Commercial Analogs Inhibit SOC-Dependent Calcium Influx

(A) SOC-mediated calcium influx quantified by ratiometric Fura-2 imaging in cells treated with 0.1% DMSO. TG application induced a transient calcium rise due to ER store depletion followed by sustained SOC-mediated calcium influx upon readdition of 2 mM calcium to extracellular medium. All error bars represent SEM.

(B–E) SOC-mediated calcium influx is reduced significantly by 50 μM AnCoA4 (B) or 50 μM AnCoF6 (C) and reduced mildly by 50 μM AnCoA5 (D), with no observed reduction by 50 μM AnCoG4 (E).

(F–I) SOC-mediated calcium influx is inhibited by analogs of AnCoA4. Compared with 0.1% DMSO (F), SOC-mediated calcium influx is significantly reduced by treatment with 50 μM AnCo4882 (G), 50 μM (+)-12a-epimilletos (H), or 50 μM biochanin A (I).

(J) AnCoA4 does not alter ER store depletion. AnCoA4 (red), AnCoF6 (orange), AnCoG4 (green), and AnCoA5 (blue) treatments do not alter calcium rise induced by TG-mediated store depletion compared with DMSO (black).

(K) Selected hits from the screen reduce the slope of SOC-dependent calcium influx. Bars represent the measured slopes from SOC calcium rise of Fura-2 imaging in (A)–(E).

(L) Analogs of AnCoA4 reduce the slope of SOC-dependent calcium influx. Bars represent the measured slope from SOC calcium rise of Fura-2 imaging in (F)–(I).

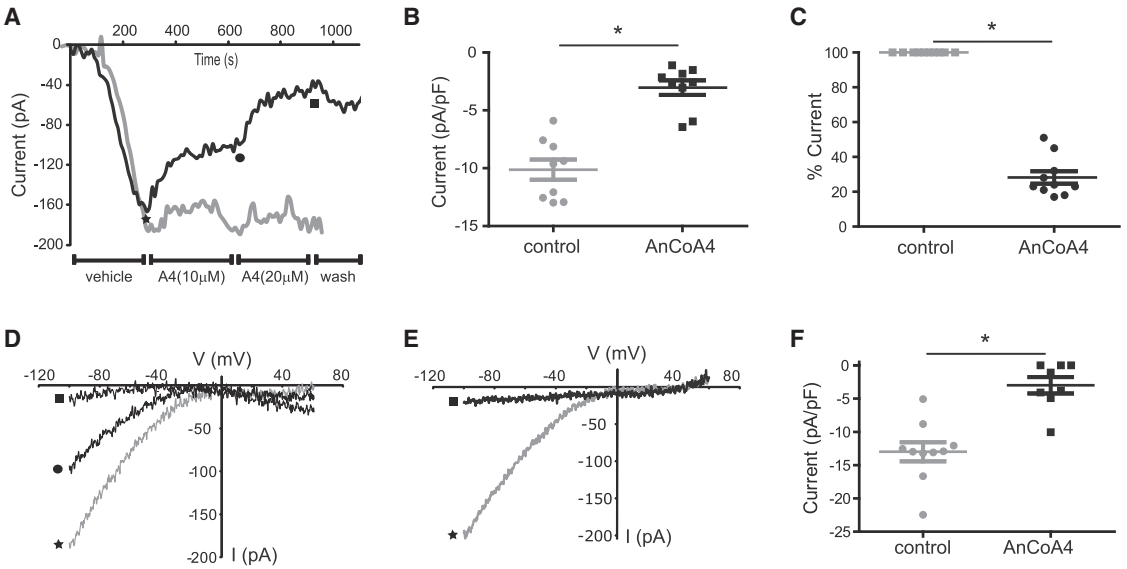

Figure 3. Electrophysiological Characterization of I_{CRAC} Inhibition by AnCoA4 in HEK293 Cells Stably Coexpressing STIM1 and Orai1

(A) AnCoA4 inhibits I_{CRAC} in a dose-dependent manner. TG-induced currents were monitored using a voltage clamp over time. DMSO (star), AnCoA4 at 10 μM (circle) and at 20 μM (square) of AnCoA4 were added at indicated time points. A representative current trace from a DMSO-treated cell is shown in gray.

(B) Acute application of 20 μM AnCoA4 significantly reduced current densities of activated channels compared with DMSO-treated control condition. Each dot represents the current amplitude measured 5 min after the addition of DMSO or AnCoA4. All error bars represent SEM.

(C) I_{CRAC} amplitude of each AnCoA4-treated cell plotted as the percentage of I_{CRAC} amplitude before the application of AnCoA4 from (B).

(D) Representative current-voltage (I-V) relationship plotted for cells acutely treated with 0.1% DMSO (star), 10 μM AnCoA4 (circle), and 20 μM AnCoA4 (square) in 2 mM calcium bath from (A). AnCoA4 shows inhibition of I_{CRAC} without affecting gating properties.

(E) Representative I-V curves from cells pretreated with 5 μM AnCoA4 (square) or 0.1% DMSO (star) for 10 min, then allowed to develop I_{CRAC} in a 2 mM calcium solution.

(F) Cells pretreated with AnCoA4 (5 μM) show markedly reduced I_{CRAC} compared with DMSO-treated control cells. Each dot represents the current amplitude recorded from a single cell. *$p < 0.01$.

We next asked whether the potency of AnCoA4 was affected by the activation state of the channel by treating cells with AnCoA4 before activation of Orai1 and then measuring the current. Although vehicle-treated cells developed up to ~200 pA of current, cells pretreated with 5 μM AnCoA4 developed no current at all (Figures 3E and 3F). Compared with the 20 μM concentration required for postactivation treatment, these results revealed a dramatic increase in potency when applied before channel activation, suggesting that AnCoA4 is more effective when it is administered before STIM1 starts interacting with Orai1.

AnCoA4 Binds Directly to Orai1

Our results strongly suggested that AnCoA4 binds and inhibits Orai1, but the exact binding site was not apparent. To address this question, we used a fluorescence aggregation assay that measures the binding of small molecules to a recombinant mCherry-fused protein. In this assay, protein aggregation quenches the mCherry fluorescence; compounds that bind to the protein increase fluorescence by preventing mCherry aggregation and quenching. We found that AnCoA4 increased the fluorescence of the C terminus of Orai1 fused to mCherry but had no effect on the N terminus or the 2-3 loop of Orai1 fused to the same protein (Figure 4A). We also used surface plasmon resonance (SPR) to measure the direct binding of AnCoA4 to different domains of Orai1 and found robust concentration-dependent binding to the C terminus of Orai1 and essentially no binding to the 2-3 loop and N terminus of Orai1 protein (Figure 4B). The apparent affinity of AnCoA4 was weaker than the EC_{50} determined in cells, possibly because the protein fragments are incompletely folded in buffer where hydrophobic plasma membrane provides additional binding affinity for the compound in the native context of the cell. Overall, these two experiments suggest that AnCoA4 binds directly to Orai1, preferentially to the C terminus.

The recent publication of the crystal structure of *Drosophila* Orai1 as well as our investigation of the structure function relationship of AnCoA4 made it possible for us to use computational methods to gain additional insights into AnCoA4 binding to Orai1(Hou et al., 2012). We used the FRED docking algorithm to look for binding sites on a homodimer of Orai1 and identified two putative binding sites (Figure 4C). One site in the main cavity encompasses a region that lacks 16 amino acids in the crystal structure, so we did not pursue it further. The second binding site for AnCoA4, however, lies in the interface between the C termini of neighboring Orai1 dimers and is composed of the polar contacts His299, Glu318, Thr312, and possible pi-pi and hydrophobic interactions with Phe300 (Figures 4D–4F). These residues are conserved in the human Orai1 protein, suggesting that this could be the binding site for the human protein. It is worth noting that AnCoA4 was not cocrystallized with Orai1, and docking only provides a potential binding site for AnCoA4. Experimental findings

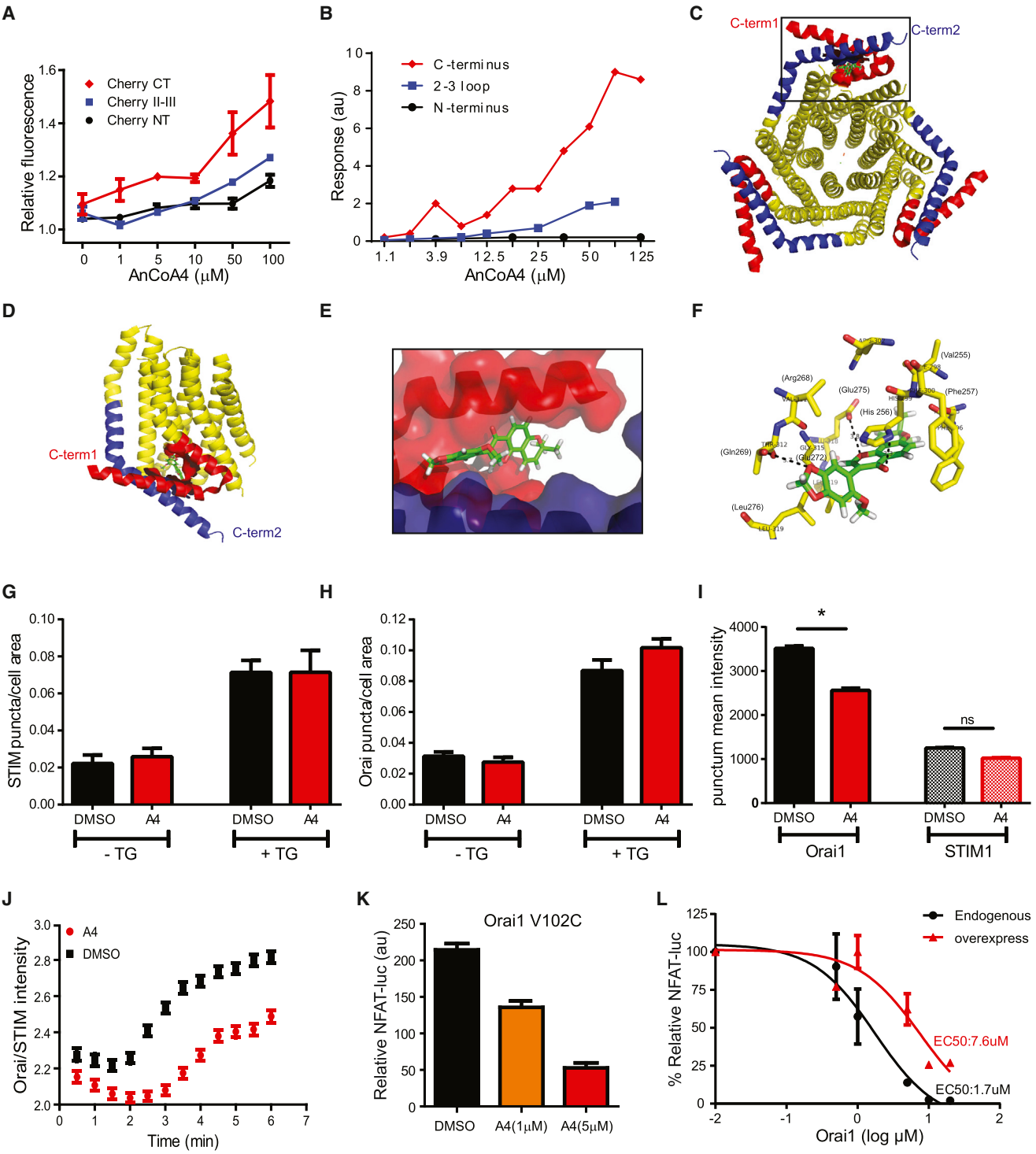

Figure 4. AnCoA4 Binds to a Single Putative Binding Site on Orai1 C Terminus and Perturbs STIM1-Orai1 Interaction

(A) AnCoA4 binds strongly to the C terminus of Orai1. Increased mCherry fluorescence represents a reduction in MFD aggregation-induced quenching. AnCoA4 significantly reduces aggregation of Orai1 C terminus but not 2-3 loop or N terminus.

(B) SPR analysis of binding of the Orai1 N terminus (black), 2-3 loop (blue), and C terminus (red) at various concentrations of AnCoA4.

(C) Architectural representation of the intracellular view of Orai1 (*D. melanogaster*) hexameric channel. Red and blue ribbons represent the putative C termini of the first and second Orai1 subunits in a single homodimer. AnCoA4 is shown in a putative binding site of only one homodimer out of three (black rectangle).

(D) Side view of a single homodimeric subunit of Orai1 with AnCoA4 putative binding site in the C-terminal arms.

(E) Zoomed-in view of putative binding of AnCoA4 in the C-terminal interface of two Orai1 Fragments.

(legend continued on next page)

suggested that these interactions are important for binding, because modifications to the central ring (ring B) of isoflavone AnCoA4 render the molecule inactive. Furthermore, highly polar groups added to ring A of AnCoA4 that interfere with hydrophobic interactions decrease the inhibition. Interestingly, in AnCoA4, the western benzodioxole group is rotated relative to the core isoflavone, which likely facilitates the other polar interaction with Gln269. Molecules with this rotation hindered such as epimilletosin show reduced potency.

We also used mutagenesis of Orai1 to identify residues involved in direct binding to AncoA4. We made over 30 mutations in the C terminus of Orai1 and investigated whether these mutations prevented inhibition of the channel by AncoA4. Two mutations, S263M and L273I, resulted in a modest reduction of AncoA4 inhibition, while the rest had either no effect or completely eliminated activation of the channel (Figure S5). Combining the two functional mutations eliminated the activity of the channel completely, so it was not possible to determine if they would have combined synergistically. These results suggest that AncoA4 is likely to bind directly to the C terminus of Orai1.

AnCoA4 Perturbs the Interaction between STIM1 and Orai1

Because the C terminus of Orai1 is an important binding site for STIM1, we asked if AnCoA4 could inhibit the binding of STIM1 to Orai1. STIM1 forms puncta and recruits Orai1 to plasma membrane ER junctions following depletion of internal calcium stores (Liou et al., 2005; Mercer et al., 2006; Zhang et al., 2005). We therefore generated a stable cell line expressing Orai1-GFP and mCherry-STIM1, depleted calcium stores using TG, and monitored the formation of puncta in presence or absence of AnCoA4 (Figure S6). Although the number of STIM1 puncta and Orai1 puncta were unchanged, we noticed a decrease in the intensity of Orai1 puncta in the presence of AnCoA4 (Figures 4G and 4H). When we quantified the fluorescence intensity of Orai1-GFP and mCherry-STIM1 in each punctum, we found that the presence of AnCoA4 did not affect the intensity of STIM1 fluorescence in puncta but significantly decreased Orai1 fluorescence intensity (Figure 4I). This change in the ratio of Orai1 to STIM1 suggested that the number of Orai1 molecules present for every STIM1 molecule is significantly lower in the presence of AnCoA4. Orai1 recruitment to STIM1 was also delayed in the presence of AnCoA4, which suggests that AnCoA4 reduces the affinity of Orai1 for STIM1 (Figure 4J).

The C terminus of Orai1 not only binds to STIM1 but also plays an important role in the opening of the channel (Frischauf et al., 2011). We therefore asked whether AnCoA4 can inhibit Orai1 independently of STIM1. We expressed a mutant of Orai1, V102C, which is constitutively active in the absence of STIM1 and treated cells with AnCoA4 (McNally et al., 2012). We found that AnCoA4 inhibited the constitutively active channel, suggesting that in addition to reducing the affinity for STIM1, AnCoA4 inhibits Orai1 directly (Figure 4K). These results are consistent with the idea that AncoA4 binds to a region of Orai1 that both controls channel gating and interacts with STIM1. To provide further confirmation for this idea, overexpression of Orai1 shifted the EC_{50} of AnCoA4 curve to the right, suggesting that AnCoA4 binds to the channel directly (Figure 4L). Additionally, overexpression of STIM1 almost completely prevented AnCoA4 inhibition of the channel, suggesting that STIM1 and AnCoA4 compete for the same binding site on Orai1 (Figure S7).

AnCoA4 Inhibits Genes Involved in T Cell Activation

The ability of AnCoA4 to potently suppress activation of an NFAT reporter gene suggests that it blocks one of the major transcriptional pathways that regulate T lymphocyte activation. To determine if AnCoA4 also suppresses the expression of relevant endogenous genes, we used quantitative RT-PCR (qRT-PCR) to measure the expression of 80 genes that play key roles in T cell activation (Figure 5A). We stimulated Jurkat T cells with phytohemagglutinin (PHA), a lectin and a commonly used activator reagent of T cells, in the presence of AnCoA4 (10 μM) and observed a downregulation of 83% of the genes associated with T cell activation. This subset included *IL2*, *IL3*, and *TNF*, as well as a number of chemokine receptor genes necessary for T cell migration and extravasation. These results indicated that AnCoA4 can inhibit the expression of endogenous genes that are required for activation of T lymphocytes.

To determine if AnCoA4 primarily affects genes that are regulated by calcium, we compared the effects of AnCoA4 with the effects of CsA, a calcineurin inhibitor. We found that AnCoA4 decreased the expression of most but not all of the same genes as CsA, including *IL2*, *CD27*, *NFATC1*, *TNF*, *TBX21*, *CSF*, *ICOS*, and *CXCR3* (Figure 5B). AnCoA4 inhibited fewer genes than CsA but suppressed other genes, such as IL18, that are unaffected by CsA exposure. These data suggest that AnCoA4 could be a more effective inhibitor than CsA in physiological processes that involve *IL18*. It also shows that molecules such as AnCoA4 and CsA could be used in combination to

(F) Stick representation of amino acids surrounding (within 4 Å) the most favorable conformation of AnCoA4 (green structure) in its putative binding site. *Drosophila* amino acids are labeled in black. Important corresponding human amino acids are labeled in parentheses.
(G) AnCoA4 treatment does not affect STIM1 puncta formation. HEK293 cells were treated with 0.1% DMSO (black, n = 7) or with 50 μM AnCoA4 (red, n = 9) at time zero, 1 min before the addition of TG. Images collected at minute 6 were then taken for analysis. All error bars represent SEM.
(H) AnCoA4 treatment does not affect Orai1 puncta formation. Cells were treated with 0.1% DMSO (black, n = 25) or with 50 μM of AnCoA4 (red, n = 24) at time zero, 1 min before the addition of TG. Images collected at minute 6 were then taken for analysis.
(I) AnCoA4 treatment reduces the number of Orai1 molecules in each puncta. Each bar represents the average of mean fluorescence intensity for each punctum (n = 820) in DMSO-treated cells and AnCoA4-treated cells (50 μM, n = 525). *$p < 0.01$. Compound treatment was performed according to protocols in (G) and (H).
(J) Cells treated with AnCoA4 exhibit a reduced number of Orai1 molecules per STIM1 molecule in each punctum (red) compared with DMSO control (black). AnCoA4 (50 μM) was added at time zero, 1 min before the addition of TG at minute 1.
(K) AnCoA4 inhibits the constitutively active Orai1 (V102C), independent of STIM1. Orai1 (V102C) activity was assayed using NFAT-luciferase assay, as in Figure 1. HEK293T cells were transfected with Orai1 (V102C) in absence of STIM1 and treated with AnCoA4.
(L) Overexpression of Orai1 shifted the EC_{50} curve relative to endogenous levels of Orai1 and rescued the inhibitory effects of AnCoA4. Log of Orai1 concentrations (log[Orai1 μM]) were used to plot and calculate EC_{50} values.

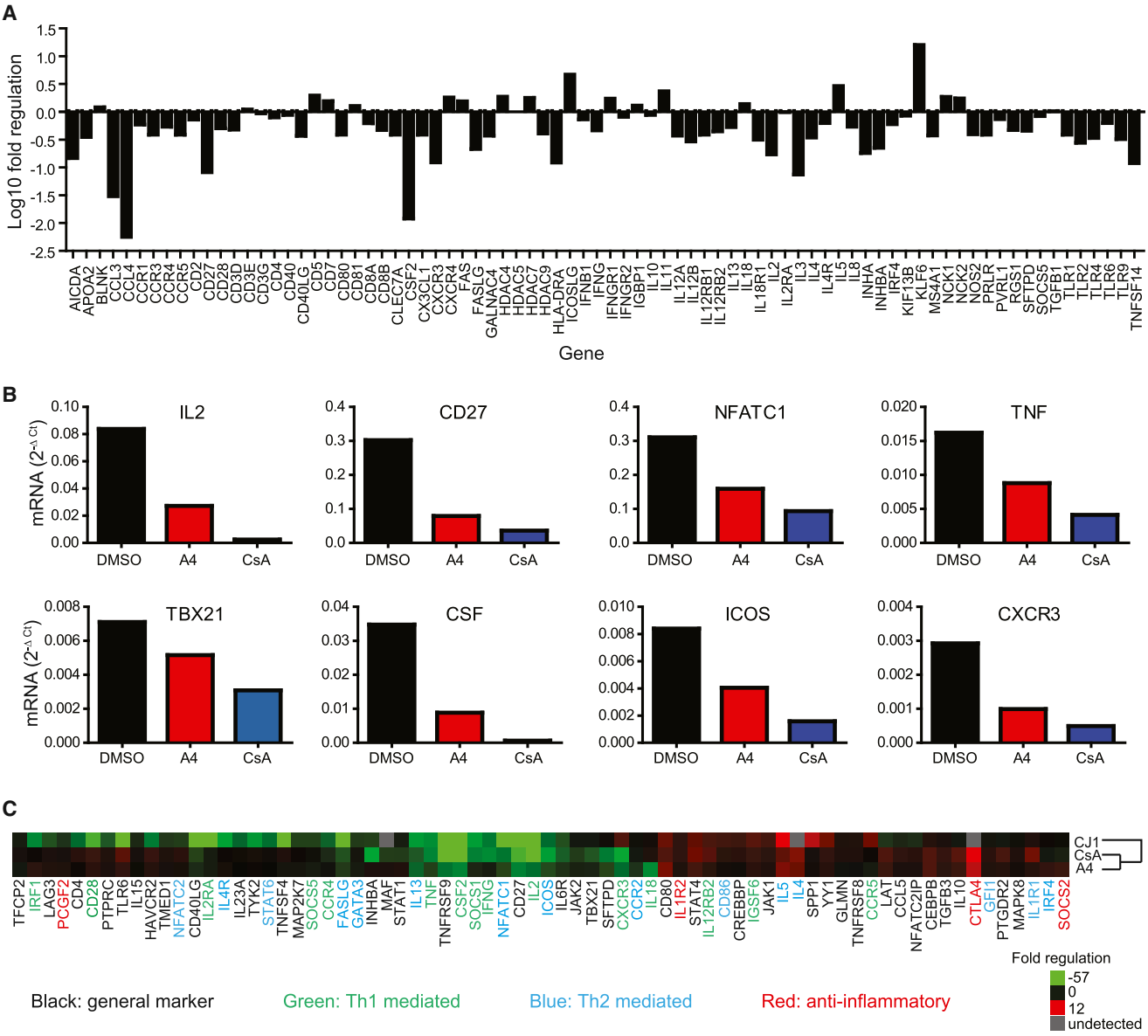

Figure 5. AnCoA4 Has a Robust Effect on Gene Expression of Activated T Cells

(A) AnCoA4 treatment effects expression of T cell activation mediating genes in Jurkat T cells. Fold change in PHA-activated induction of genes for AnCoA4-treated cells over DMSO-treated control is plotted.

(B) AnCoA4 treatment downregulates known T cell-activating genes. Compared with DMSO-treated cells (black), treatment with AnCoA4 (10 μM) (red) and CsA (50nM) (blue) reduced mRNA levels of T cell-activating genes.

(C) AnCoA4 and CsA have similar effects on gene expression. Gene expression heatmap of 10 μM AnCoA4-treated (bottom row) and 50 nM CsA-treated (middle row) Jurkat T cells. The gene profile of SOC-deficient Jurkat T cells (CJ1, top row) is shown for comparison. Green and red colors indicate down- and upregulation, respectively. Assayed genes include general markers of T cell activation (black), Th1-affiliated (green) and Th2-affiliated (blue) genes, and putative immunosuppressive genes (red).

produce more robust therapeutics effects for appropriate medical conditions.

We next compared the gene expression profile of cells treated with AnCoA4 and the gene expression profile of the CJ1 Jurkat T cell line, which lacks a functional STIM1 protein and therefore SOC (Figure 5C) (Park et al., 2010). Knockout of STIM1 reduced the expression of approximately twice as many genes as AnCoA4 or CsA, indicating that a complete abolishment of SOC has a much broader impact on T cell activation and function.

AnCoA4 Effectively Inhibits the Immune Response in Vitro and in Vivo

The ability of AnCoA4 to reduce the expression of genes that participate in T cell activation suggests that it may be an effective immunosuppressant. To test this idea directly, we used the

mixed lymphocyte reaction (MLR), in which fluorescently labeled lymphocytes of one strain of mouse are mixed with lymphocytes (irradiated splenocytes) of an allogeneic mouse strain in vitro. In this assay, exposure of T cells to allogeneic cells triggers cell proliferation that can be monitored by measuring the dilution of fluorescently labeled cells as they divide (Figure 6A). Treatment of the proliferating cells with either 10 or 50 μM of AnCoA4 twice a day for 7 days inhibited cell proliferation by 90% relative to control. This is similar to what is observed with treatment of CsA, with the caveat that CsA is more potent than AnCoA4 (Figure 6B; see Table S1 for p values). Interestingly AnCoA4 seemed to be somewhat more persistent than CsA in cell culture, probably because of its hydrophobicity.

To examine the effect of AnCoA4 in vivo, we used a modified ovalbumin-induced, delayed-type hypersensitivity (DTH) model (Black, 1999; Lamont et al., 1989; Müller et al., 2002). In this model, animals are primed by dorsal subcutaneous injection of complete Freund's adjuvant (CFA) mixed with ovalbumin (ova). Three days later, mice are challenged with ova with or without incomplete Freund's adjuvant (IFA) by injection into the footpad. This local exposure of ova results in the proliferation of lymphocytes, particularly in the popliteal lymph nodes, which are harvested and analyzed after six days (see Experimental Procedures).

Mice were injected intravenously with or without AnCoA4 4 hr before and three injections after the test injection of ova into the footpad. All mice appeared to tolerate the drug well, showing no apparent indications of sickness or acute toxicity throughout the 6 days of the experiment. Harvesting of the popliteal lymph nodes showed that mice treated with AnCoA4 and CsA had significantly smaller popliteal lymph nodes than vehicle-treated animals (Figure 6C). Quantification of these results confirmed that both AnCoA4 and CsA decreased the cellularity of lymph nodes consistent with their role as immunosuppressant agents in vivo (Figure 6D).

We designed a second study to determine if AnCoA4 could prevent T cell activation without pretreatment of the animal (Figure 6E). Histological evaluation of the footpads showed that vehicle-injected mice had a robust local inflammatory response involving both the footpad and underlying structures. This response consisted of both primary lymphohistiocytic inflammation and extensive secondary neutrophil infiltration and tissue damage (Figures 6F and 6G). AnCoA4-treated animals showed a greatly reduced lymphohistiocytic inflammation with no neutrophil and tissue damage (Figures 6H and 6I) and blind scoring of the histological sections confirmed that both AnCoA4 and CsA reduced the degree of local inflammation in OVA-injected footpads. In contrast, local injection of IFA in the footpad caused a robust innate immune response that was not blocked by AnCoA4 or CsA, indicating that these two immunosuppressant agents could have the potential to selectively block T cell-mediated responses (Figure 6J). Further studies are needed to fully characterize the specific effects of AnCoA4 on different classes of immune cells, but it is clear from our studies that AnCoA4 can inhibit T cell activation and proliferation in vivo.

DISCUSSION

In this study, we identified a small-molecule blocker for SOC channels by taking advantage of the structural knowledge gained by studying its two major constituents, STIM1 and Orai1. By using MFDs of Orai1 and STIM1 to search for molecules that bind to the functional domain of the channel, we identified 4 compounds from a collection of 12,000 that were capable of inhibiting Orai1. One of these compounds, AnCoA4, binds directly to the C terminus of Orai1, blocks the expression of calcium-regulated genes that control T cell activation and inhibits T cell-mediated immune responses in vivo. Blockers of SOC channels, and of Orai1 in particular, are promising for a number of therapeutic areas, including immunomodulation, inflammation, and thrombosis. A clear understanding of the mechanism of action and binding site of AnCoA4, along with its ability to inhibit T cell activation in vitro and in vivo, makes it a useful new tool for studying the role of CRAC channels in the immune system. Our knowledge of the mechanism of action of AnCoA4 has already proved useful for the rational design of more effective analogs with improved potency and specificity.

Our characterization of AnCoA4 provides interesting insights into the mechanism of CRAC channel activation. The C terminus is an established target for Orai1; however, the N terminus also binds to STIM1 and is important for gating and activation of the channel. By binding directly to the C terminus of Orai1, AnCoA4 effectively blocks the channel and inhibits recruitment of STIM1. AnCoA4 appears to work more efficiently when applied prior to the recruitment of STIM1 to Orai1, suggesting that it competes with STIM1 for a binding site on the C terminus of the channel. More surprisingly, AnCoA4 can inhibit Orai1 activation even in the absence of STIM1, as indicated by its ability to inhibit a constitutively active channel. These findings suggest that AnCoA4 and STIM1 bind to similar regions of the C terminus of Orai1.

AnCoA4 was also effective at inhibiting DTH reaction in vivo. Because of its low solubility, it had to be formulated such that it would not precipitate upon injection. This low solubility, along with its chemical stability, had the unexpected benefit of providing long-lasting immunosuppression over a period of days. Despite this long-lasting effect, AnCoA4 was not toxic to animals even at high doses.

Importantly, we identified AnCoA4 using a method for drug discovery that, until now, had not been applied to ion channels. Historically, small-molecule screens for ion channel blockers have used heterologous cell lines expressing nonphysiological levels of ion channels, combined with intracellular calcium dyes to measure the activity of the channel. Although this approach has been as effective, it also presents some practical challenges. As a first-line approach, cell-based assays are resource intensive and yield a large number of off-target hits. This process then requires follow-up studies to characterize and validate all hits, which makes the process somewhat cumbersome and expensive. Because the molecular target and mechanism of action of compounds identified in cell-based assays are often unknown, structural activity based optimization of these compounds using traditional medicinal chemistry has been challenging. Cell-based assays also tend to exclude potentially useful lead compounds that could bind to intracellular regions of a channel but have low cell permeability or low affinity.

In this study, we developed a cell-free method to screen thousands of compounds for their ability to bind to functional

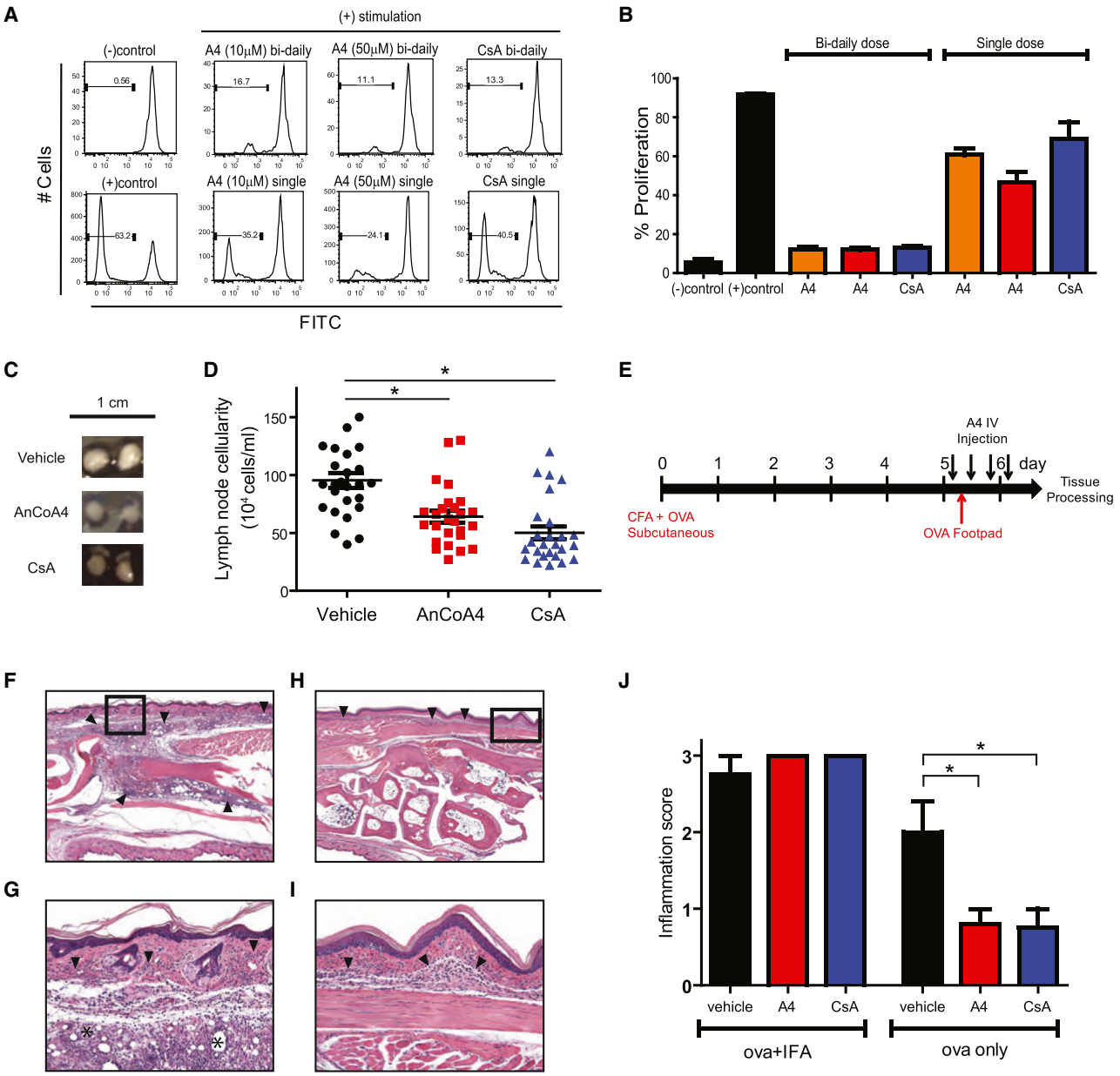

Figure 6. AnCoA4 Inhibits T Cell Responses in MLR and In Vivo DTH Model

(A) AnCoA4 inhibits proliferation in MLR. FACS plots of proliferating T cells labeled with CFSE, a plasma membrane-labeling dye, are shown. Cells in (-)control were not stimulated (top left), whereas cells in (+)control were stimulated with irradiated allogeneic splenocytes. Treatment conditions are shown above each FACS plot.

(B) Summary of effect of AnCoA4 on mixed lymphocyte proliferation from (A). Cells stimulated with allogeneic splenocytes were treated with 10 μM of AnCoA4 (orange), 50 μM of AnCoA4 (red), and 50 nM of CsA. Each bar represents the quantification of percentage proliferation by indicated dose regimen. All error bars represent SEM.

(C and D) AnCoA4 treatment reduces lymphocyte proliferation in vivo. Dissected popliteal lymph nodes from vehicle-treated (top), AnCoA4-treated (middle), and CsA-treated (bottom) mice are shown (C). AnCoA4 treatment reduces the node size as well as number of cells per lymph node (D). Each dot represents one lymph node (see Experimental Procedures).

(E) Schematic of AnCoA4 and ova injection schedule for in vivo DTH studies.

(F–I) AnCoA4 treatment attenuates local inflammatory response. Histological representation of paw cross-sections stained with hematoxylin and eosin. Vehicle-injected mice exhibit a robust local inflammatory response involving the foot pad and underlying structures (black arrowheads, F). A magnified representation of the black square from (F) shows primary lymphohistiocytic inflammation (arrowheads) with extensive secondary neutrophil infiltration with tissue damage (asterisks, G). AnCoA4 treatment leads to a greatly attenuated response limited only to the footpad (black arrowheads, H), with only moderate lymphohistiocytic inflammation and no or minimal secondary neutrophil accumulation apparent in magnified view (I).

(J) Histological scoring of foot pad inflammation. Each bar represents histological grading for a single treatment containing paws from four or five mice per group (see Experimental Procedures). *$p < 0.05$.

regions of Orai1 and STIM1. As structural information about ion channels is now widely available, it should be possible to design screens to target not only specific ion channels but specific functions of ion channels that are mediated by specific domains. A potential limitation of our approach is that channel fragments may not fold into their native tertiary structure in solution and thus might not behave as in the intact channel. We mitigated this risk by selecting the CAD and the C terminus of Orai1, both of which can modulate the activity of the channel when introduced into intact cells (Mullins et al., 2009; Park et al., 2009). This method therefore provides us with the ability to screen for compounds inexpensively and quickly, resulting in hits where a known binding site and mechanism of action can facilitate structural optimization.

SIGNIFICANCE

SOC entry is required for activation of immune cells, and its lack of function causes SCID in human patients. In lymphocytes, this process is mediated through the Orai family of calcium channels, which are activated by direct binding to STIM proteins that act as calcium sensors in ER. SOC has recently been shown to play a major role in several other physiological and pathological processes, ranging from muscle development to cancer. It is now clear that SOC components are ubiquitously expressed in variety of tissues, severing diverse functions. Abnormal overactivation of immune response causes autoimmune disorders, and the lack of safe and long-term treatments has created the need for novel and improved immunosuppressant agents. Pharmacological blockers of SOC channels provide us with tools to further examine the physiological role of SOC and could ultimately allow the development of potential treatments of autoimmune disorders. We have designed a platform methodology for generating SOC blockers on the basis of identification and targeting MFDs of STIM1 and Orai1. AnCoA4, a small-molecule blocker that inhibits SOC at submicromolar concentrations, was identified using this methodology. AnCoA4 binds directly to the C terminus of Orai1 and blocks calcium influx independent of binding to STIM1. It also reduces the affinity of STIM1 for Orai1 and inhibits T cell activation both in vitro and in vivo. AnCoA4 confers selectivity to Orai1 over L-type calcium channels, but further examination of specificity is required to understand the off-target liabilities of this molecule. This process, coupled with medicinal chemistry and structural-activity relationship studies, could result in lead molecules for development of useful clinical reagents.

EXPERIMENTAL PROCEDURES

Composite *Z* Score Calculation

Median values were calculated for all mock spots on each SMM to produce a trimmed mock distribution population. The mean of the trimmed mock distribution was then subtracted from each sample spot on the same SMM to produce background subtracted values. These values were then divided by twice the SD of the trimmed mock measurements to give *Z* scores. Cosine correlation analysis of *Z* scores was then used to determine a composite *Z* score for each sample spot.

Protein Expression and SMM

All fusion proteins (Orai1-NT [1–91], II-III loop [142–177], CT [255–301], and STIM1-CAD128 [342–469]) used for screens and binding assay were constructed in pGEX6p plasmids (Invitrogen) transformed, produced, and purified from BL21 bacteria according to the manufacturer's instructions. SMMs were screened and data were analyzed according protocols described previously in collaboration with the Broad Institute (Seiler et al., 2008; Vegas et al., 2008).

Cells and Transfection

HEK293 and HEK293T cells (ATCC) were cultured in Dulbecco's modified Eagle's medium (DMEM) with GlutaMax (GIBCO), 10% fetal bovine serum (Hyclone). A HEK293 cell line with an inducible mcherry-STIM1-T2A-Orai1-eGFP and mcherry-STIM1-T2A-myc-Orai1 were generated with the T-REx system (Invitrogen) and were maintained with 100 μg/ml hygromycin. Cells were transfected at 90% confluency with 0.2 to 0.5 μg DNA using Lipofectamine 2000 (Invitrogen) according to the manufacturer's instructions.

NFAT-Luciferase Assays

HEK293T cells were cotransfected with the indicated constructs and an NFAT reporter gene (firefly luciferase gene C-terminal to a 4X-NFAT site from the IL-2 gene). Cotransfection with the *Renilla* luciferase gene (pRLTK) driven by the TK promoter was used to control for cell number and transfection efficiency. After 12 to 18 hr, cells were treated with a control DMSO solution (mock), phorbol 12-myristate 13-acetate (PMA; 1 μM), or PMA + TG (1 μM) for 6 hr. Assays were performed with the Dual Luciferase Reporter Assay System (Promega). For each condition, luciferase activity was measured with four samples taken from duplicate wells with a 96-well automated luminometer (Turner Biosystems). Results are represented as the ratio of firefly to *Renilla* luciferase activity.

MTT RBL Viability Assay

RBL cells were plated in 96-well plates at 10,000 cells per well (100 μl/well). Twenty-four hours later, DMSO (2%, vehicle control) and AnCoA4 compound at the indicated concentrations were added in 3 wells (100 μl/compound or DMSO). Twenty-four hours later, 20 μl of MTT (0.5 mg/mL, thiazolyly blue tetrazolium bromide, Sigma, M5655) was added to each cell media for 4 hr. Two hundred microliters of 100% DMSO was added in each well. Cell lysates was measured with Microplate Reader (SpectraMax 190, Molecular Devices) at 595 nm. Background was subtracted. The percentage of cell survival was calculated using the following formula: cell survival (%) = (absolute of compound/absolute of control) × 100. Three replicate wells were measured at each compound concentration and experiments were performed at least three times.

Confocal Microscopy

HEK293 cells were plated onto sterilized coverslips coated with poly-D-lysine and transfected and maintained in complete DMEM for 12 to 18 hr before imaging in Tyrode's solution, containing 129 mM NaCl, 5 mM KCl, 2 mM CaCl2, 1 mM MgCl2, 30 mM D-glucose, and 25 mM Na-HEPES (pH 7.4). For depletion of stores, cells were treated with 1 μM TG Tyrode's solution for 6 min. Fluorescence emission was collected at 610 nm (mCherry) and 530 nm (eGFP). All experiments were performed at 22C° to 25C°. Images were collected with the UltraVIEW VoX confocal microscope (PerkinElmer) using a-plan Apochromat 63x/NA1.4 oil immersion objective and analyzed using Volocity 5 software (Improvision). To measure total puncta area per cell, punctum was defined as any clusters with normalized SDs higher than the background intensity whose size was limited to larger than 0.2 and smaller than 5 μm in area. The sum of the area of all puncta was then divided by each cell's area. To measure empirical ratio of Orai1 to STIM1 molecules, each punctum was picked manually as a region of interest, and the fluorescence of Orai1 and STIM1 was measured within that punctum over time.

Fura-2 Calcium Imaging

Cells were loaded at 37°C in DMEM with 1 μM fura-2 AM for 30 min. Ratiometric Ca^{2+} images were collected with a Nikon Eclipse 2000-U inverted microscope using Open Lab 5 software (Improvision) and analyzed using Igor Pro 6 software (Wavemetrics).

Electrophysiology

HEK293 cells expressing equimolar levels of mCherry-STIM1 and myc-Orai1 were induced and incubated by tetracycline for 14 to 18 hr in DMEM. Currents were recorded via standard whole-cell patch-clamp techniques (Prakriya and Lewis, 2001). Pipettes of resistance 3 to 5 MΩ were filled with an internal solution containing 150 mM Cs aspartate, 8 mM MgCl2, 10 mM EGTA, and 10 mM HEPES (pH 7.2 with CsOH). Currents were sampled at 5 kHz and filtered at 2 kHz, and all voltages were corrected for the junction potential of the pipette solution relative to Ringer's in the bath (−13 mV).

SPR

Orai1-NT (48–91), 2-3 loop (142–177), CT (255–301), the polypeptides were used as an immobilized ligand and dissolved in 10 mM sodium acetate buffer (pH 5.0). PBS (1×, 10 mM PO_4, 138 mM NaCl, 2.4 mM KCl, pH 7.4) was prepared from 10 × PBS for molecular interaction affinity and solvent correction. HBS-EP (HEPES buffered saline with 3mM EDTA and 0.005% surfactant P20 [BR-1001-88, Biacore]) and amine coupling reagents (400mM 1-ethyl-3-[3-dimethylamino-propyl] carbodiimide hydrochloride [EDC, a part of BR-1000-50], 100 mM N-hydroxysuccinimide [NHS, a part of BR-1000-50]), and 1M Ethanolamine-HCl (a part of BR-1000-50), 10 mM sodium acetate buffer (pH 4.0–5.5, BR-1003-49) were purchased from GE Healthcare. NaOH (50 mM) was used for regeneration.

The interactions of AnCoA4 with immobilized Orai1 C terminus were studied by using a Biacore T200 instrument (GE Healthcare). A Sensor S CM5 chips (BR-1005-30) with carbomethylated dextran covalently attached on the gold surface was purchased from GE Healthcare.

A flow cell number 2 of a sensor S CM5 chip was first activated by 400 mM EDC/100 mM NHS and then polypeptide (20 μg/ml) was immobilized by amine coupling. After washing, a chip was blocked by ethanolamine. In order to do a binding affinity analysis, AnCoA4 (0, 3.9, 15.625, 31.25, and 125 μM) was evaluated with polypeptide immobilized on the flow cell 2 as sample and on the flow cell 1 as reference using BIAevaluation software (Biacore). The sensor chip surface was regenerate by 50 mM NaOH regeneration buffer after each cycle. All experiments were repeated three times. Polypeptide sequences are described below. Human Orai1 NT amino acid (48–91): SAVTYPDWIGQ SYSEVMSLNEHSMQALSWRKLYLSRAKLKASS. Human Orai1 2-3 loop amino acid (142–177): TCILPNIEAVSNVHNLNSVKESPHERMNRHIELAWA. Human Orai1 C terminus amino acid (255–301): VHFYRSLVSHKTDRQFQEL NELAEFARLQDQLDHRGDHPLTPGSHYA. Human STIM1-CAD128 (342–469): MYAPEALQKWLQLTHEVEVQYYNIKKQNAEKQLLVAKEGAEKIKKKRNT LFGTFHVAHSSSLDDVDHKILTAKQALSEETAALRERLHRWQQIEILCGFQIVN NPGIHSLVAALNIDPSWMGSTRPNPA.

Docking

The crystal structure of Orai1 calcium channel from *Drosophila melanogaster* was obtained from the Research Collaboratory for Structural Bioinformatics Protein Data Bank (accession number 4HKR). Orai1 is a trimer of homodimers, and the asymmetric unit of the homodimer is reported in the crystal structure. Using MacPyMol, the C terminus of both chains of the asymmetric unit was extracted (beginning with residue I291), to better represent the experimental system, and this fragment of the protein was used for further study. The extracted portion of 4HKR was then loaded into the receptor generation program Make_Receptor from OpenEye Scientific, and, as the specific binding site was unknown, the protein surface was analyzed for concavity to determine potential binding sites (using the "molecular" probe). One large potential binding site was identified, and the docking receptor was built using default parameters to represent this binding site. Before docking, conformers of the ligand AnCoA4 were generated with default parameters using the conformer generation program Omega (OpenEye Scientific). This database of conformers was then docked into the previously generated receptor using the docking program FRED (OpenEye Scientific), with 20 poses being returned and otherwise default parameter usage. The top-scoring pose was selected for discussion, and potential intermolecular interactions between Orai1 and this pose were highlighted with MacPyMol.

qRT-PCR

mRNA was isolated from Jurkat T cells using RNeasy mini kit (Qiagen). First-strand cDNA and qRT-PCR was then performed using RT Profiler PCR Array Systems (SABiosciences) according to the manufacturer's instructions. Analysis and presentation were performed using Prism software (GraphPad) Cluster and TreeView software.

MLR

CD4/CD8 conventional T cells (Tcon) were prepared from splenocytes and peripheral lymph node cells and enriched with anti-CD4 MACS (Miltenyi Biotec) and then anti-CD8 MACS; purity was determined by fluorescence-activated cell sorting (FACS) on a LSR II or FACS Aria (BD Biosciences), and cells were mixed so that CD4/CD8 = 2:1. C57BL/6J Tcon (2×10^5) were labeled with carboxyfluorescein succinimidyl ester (CFSE; Invitrogen) and added to a 96-well flat-bottom plate containing complete RPMI (Invitrogen) containing 10% fetal calf serum, 2 mM L-glutamine, 100 U/ml penicillin, 100 μg/ml streptomycin (Invitrogen), and 5 μg/mL 2-mercaptoethanol (Sigma-Aldrich). For stimulation of Tcon, 10^6 BALB/c RBC-lysed splenocytes, which had received 30 Gy irradiation, were added. Total volume per well was 200 μl. After culture at 37°C and 5% CO_2 for 7 days, cells were resuspended and analyzed for proliferation by CFSE dilution on a LSR II (Becton Dickinson).

In Vivo Mouse Model of DTH

For Figures 6C and 6D, Balb/c mice were immunized subcutaneously with 50 μg of ovalbumin (Sigma) emulsified with CFA at a 1:1 ratio. Total volume of injection was 50 μl. Mice were then injected intravenously with 5 mg/kg of AnCoA4 per injection, at 3 × 50 μl/day for 3 days. Vehicle was composed of 80% PBS, 15% DMSO, and 5% 2-hydroxypropyl-betacyclodextran (Sigma). Ten microliters of emulsified IFA containing 15 ug of ovalbumin was injected in the footpad of each mouse on day 4. Intravenous dosage of AnCoA4 was at this point increased to 25 μM at 3 × 50 μl per day (75 mg/kg/day) in 20% DMSO, 10% 2-hydroxypropyl-betacyclodextran, 10% benzyl alcohol, and 60% polyethylene glycol (PEG). Mice were sacrificed and appropriate tissues harvested on day 6.

For Figures 6F to 6J, Balb/c mice were immunized subcutaneously with 50 ug of ovalbumin (Sigma) emulsified with CFA at a 1:1 ratio. Total volume of injection was 50 μl. To monitor innate immunity, 10 μl emulsified IFA containing 15 μg of ovalbumin was injected in the footpad of each mouse 5 days later. A different group was injected with 30 ug of ovalbumin only at the same time to monitor T cell-mediated response. No pretreatment of AnCoA4 starting day 3 was applied in this study, because pf limited availability of AnCoA4. AnCoA4 (25 μM) was injected intravenously at 3 × 50 μl/day (75 mg/kg/day) in 20% DMSO, 10% 2-hydroxypropyl-betacyclodextran, 10% benzyl alcohol, and 60% PEG starting on day 5, as shown in Figure 6E. Mice were sacrificed, and appropriate tissues were harvested on day. Histological inflammation scoring was determined according to the following guidelines: (1) presence of primary lymphohistiocytosis, (2) primary lymphohistiocytosis and secondary neutrophil infiltration, and (3) primary lymphohistiocytosis, secondary neutrophil leakage, and tissue damage. All animal protocols were approved by the Stanford Administrative Panel on Laboratory Animal Care, and the procedures were performed in accordance to their guidelines.

SUPPLEMENTAL INFORMATION

Supplemental Information includes seven figures and one table and can be found with this article online at http://dx.doi.org/10.1016/j.chembiol.2014.08.016.

AUTHOR CONTRIBUTIONS

A.M.S., C.Y.P., and R.E.D. conceived and designed experiments. C.Y.P. performed experiments related to Figures 1A to 1C. O.M.M. manufactured SMMs and performed analysis for Figures 1B and 1C. D.B.L.-G. performed experiments related to Figures 6A and 6B. A.N.K. performed analysis related to Figures 1B and 1C. J.I.O. provided advice and performed analysis for Figures 6F to 6J. P.N. performed analysis for Figure 4C. A.M.S. performed experiments and analysis for all other figures. A.M.S., C.Y.P., and R.E.D. wrote the manuscript.

ACKNOWLEDGMENTS

This work was supported by NIH grants DP1OD003889 and R21MH087898, the Simons Fund for Autism Research, California Institute for Regenerative Medicine grant TG 01159 and in part by funds from the National Cancer Institute's Initiative for Chemical Genetics (contract N01-CO-12400), the National Research Foundation of Korea (MEST) NRF-2012-R1A1-A1044814, and by a grant from Future Challenge Project funded by the Ulsan National Institute of Science and Technology (1.120050.01). The content of this publication does not necessarily reflect the views or policies of the US Department of Health and Human Services, nor does the mention of trade names, commercial products, or organizations imply endorsement by the US government. We would like to thank Daria Mochly-Rosen, Kevin Grimes, the SPARK translational program, and the Office of Technology and Licensing at Stanford University for funding and guidance throughout the process. We would also like to thank A. Nigh for feedback on the manuscript.

Received: November 20, 2013
Revised: August 3, 2014
Accepted: August 5, 2014
Published: October 9, 2014

REFERENCES

Black, C.A. (1999). Delayed type hypersensitivity: current theories with an historic perspective. Dermatol. Online J. *5*, 7.

Burdmann, E.A., Andoh, T.F., Yu, L., and Bennett, W.M. (2003). Cyclosporine nephrotoxicity. Semin. Nephrol. *23*, 465–476.

Chen, G., Panicker, S., Lau, K.Y., Apparsundaram, S., Patel, V.A., Chen, S.L., Soto, R., Jung, J.K., Ravindran, P., Okuhara, D., et al. (2013). Characterization of a novel CRAC inhibitor that potently blocks human T cell activation and effector functions. Mol. Immunol. *54*, 355–367.

Diver, J.M., Sage, S.O., and Rosado, J.A. (2001). The inositol trisphosphate receptor antagonist 2-aminoethoxydiphenylborate (2-APB) blocks Ca2+ entry channels in human platelets: cautions for its use in studying Ca2+ influx. Cell Calcium *30*, 323–329.

Feng, M., Grice, D.M., Faddy, H.M., Nguyen, N., Leitch, S., Wang, Y., Muend, S., Kenny, P.A., Sukumar, S., Roberts-Thomson, S.J., et al. (2010). Store-independent activation of Orai1 by SPCA2 in mammary tumors. Cell *143*, 84–98.

Feske, S. (2007). Calcium signalling in lymphocyte activation and disease. Nat. Rev. Immunol. *7*, 690–702.

Feske, S. (2009). ORAI1 and STIM1 deficiency in human and mice: roles of store-operated Ca2+ entry in the immune system and beyond. Immunol. Rev. *231*, 189–209.

Feske, S. (2010). CRAC channelopathies. Pflugers Arch. *460*, 417–435.

Feske, S., Gwack, Y., Prakriya, M., Srikanth, S., Puppel, S.H., Tanasa, B., Hogan, P.G., Lewis, R.S., Daly, M., and Rao, A. (2006). A mutation in Orai1 causes immune deficiency by abrogating CRAC channel function. Nature *441*, 179–185.

Frischauf, I., Muik, M., Derler, I., Bergsmann, J., Fahrner, M., Schindl, R., Groschner, K., and Romanin, C. (2009). Molecular determinants of the coupling between STIM1 and Orai channels: differential activation of Orai1-3 channels by a STIM1 coiled-coil mutant. J. Biol. Chem. *284*, 21696–21706.

Frischauf, I., Schindl, R., Bergsmann, J., Derler, I., Fahrner, M., Muik, M., Fritsch, R., Lackner, B., Groschner, K., and Romanin, C. (2011). Cooperativeness of Orai cytosolic domains tunes subtype-specific gating. J. Biol. Chem. *286*, 8577–8584.

Gwack, Y., Feske, S., Srikanth, S., Hogan, P.G., and Rao, A. (2007). Signalling to transcription: store-operated Ca2+ entry and NFAT activation in lymphocytes. Cell Calcium *42*, 145–156.

Hogan, P.G., Lewis, R.S., and Rao, A. (2010). Molecular basis of calcium signaling in lymphocytes: STIM and ORAI. Annu. Rev. Immunol. *28*, 491–533.

Hoorn, E.J., Walsh, S.B., McCormick, J.A., Fürstenberg, A., Yang, C.L., Roeschel, T., Paliege, A., Howie, A.J., Conley, J., Bachmann, S., et al. (2011). The calcineurin inhibitor tacrolimus activates the renal sodium chloride cotransporter to cause hypertension. Nat. Med. *17*, 1304–1309.

Hoth, M., and Penner, R. (1992). Depletion of intracellular calcium stores activates a calcium current in mast cells. Nature *355*, 353–356.

Hou, X., Pedi, L., Diver, M.M., and Long, S.B. (2012). Crystal structure of the calcium release-activated calcium channel Orai. Science *338*, 1308–1313.

Lamont, A.G., Mowat, A.M., and Parrott, D.M. (1989). Priming of systemic and local delayed-type hypersensitivity responses by feeding low doses of ovalbumin to mice. Immunology *66*, 595–599.

Lewis, R.S., and Cahalan, M.D. (1989). Mitogen-induced oscillations of cytosolic Ca2+ and transmembrane Ca2+ current in human leukemic T cells. Cell Regul. *1*, 99–112.

Liou, J., Kim, M.L., Heo, W.D., Jones, J.T., Myers, J.W., Ferrell, J.E., Jr., and Meyer, T. (2005). STIM is a Ca2+ sensor essential for Ca2+-store-depletion-triggered Ca2+ influx. Curr. Biol. *15*, 1235–1241.

McCarl, C.A., Picard, C., Khalil, S., Kawasaki, T., Röther, J., Papolos, A., Kutok, J., Hivroz, C., Ledeist, F., Plogmann, K., et al. (2009). ORAI1 deficiency and lack of store-operated Ca2+ entry cause immunodeficiency, myopathy, and ectodermal dysplasia. J. Allergy Clin. Immunol. *124*, 1311–1318.e7.

McCarl, C.A., Khalil, S., Ma, J., Oh-hora, M., Yamashita, M., Roether, J., Kawasaki, T., Jairaman, A., Sasaki, Y., Prakriya, M., and Feske, S. (2010). Store-operated Ca2+ entry through ORAI1 is critical for T cell-mediated autoimmunity and allograft rejection. J. Immunol. *185*, 5845–5858.

McNally, B.A., Somasundaram, A., Yamashita, M., and Prakriya, M. (2012). Gated regulation of CRAC channel ion selectivity by STIM1. Nature *482*, 241–245.

Mercer, J.C., Dehaven, W.I., Smyth, J.T., Wedel, B., Boyles, R.R., Bird, G.S., and Putney, J.W., Jr. (2006). Large store-operated calcium selective currents due to co-expression of Orai1 or Orai2 with the intracellular calcium sensor, Stim1. J. Biol. Chem. *281*, 24979–24990.

Muik, M., Frischauf, I., Derler, I., Fahrner, M., Bergsmann, J., Eder, P., Schindl, R., Hesch, C., Polzinger, B., Fritsch, R., et al. (2008). Dynamic coupling of the putative coiled-coil domain of ORAI1 with STIM1 mediates ORAI1 channel activation. J. Biol. Chem. *283*, 8014–8022.

Müller, G., Müller, A., Tüting, T., Steinbrink, K., Saloga, J., Szalma, C., Knop, J., and Enk, A.H. (2002). Interleukin-10-treated dendritic cells modulate immune responses of naive and sensitized T cells in vivo. J. Invest. Dermatol. *119*, 836–841.

Mullins, F.M., Park, C.Y., Dolmetsch, R.E., and Lewis, R.S. (2009). STIM1 and calmodulin interact with Orai1 to induce Ca2+-dependent inactivation of CRAC channels. Proc. Natl. Acad. Sci. U S A *106*, 15495–15500.

Oh-Hora, M., Yamashita, M., Hogan, P.G., Sharma, S., Lamperti, E., Chung, W., Prakriya, M., Feske, S., and Rao, A. (2008). Dual functions for the endoplasmic reticulum calcium sensors STIM1 and STIM2 in T cell activation and tolerance. Nat. Immunol. *9*, 432–443.

Park, C.Y., Hoover, P.J., Mullins, F.M., Bachhawat, P., Covington, E.D., Raunser, S., Walz, T., Garcia, K.C., Dolmetsch, R.E., and Lewis, R.S. (2009). STIM1 clusters and activates CRAC channels via direct binding of a cytosolic domain to Orai1. Cell *136*, 876–890.

Park, C.Y., Shcheglovitov, A., and Dolmetsch, R. (2010). The CRAC channel activator STIM1 binds and inhibits L-type voltage-gated calcium channels. Science *330*, 101–105.

Prakriya, M., and Lewis, R.S. (2001). Potentiation and inhibition of Ca(2+) release-activated Ca(2+) channels by 2-aminoethyldiphenyl borate (2-APB) occurs independently of IP(3) receptors. J. Physiol. *536*, 3–19.

Roos, J., DiGregorio, P.J., Yeromin, A.V., Ohlsen, K., Lioudyno, M., Zhang, S., Safrina, O., Kozak, J.A., Wagner, S.L., Cahalan, M.D., et al. (2005). STIM1, an essential and conserved component of store-operated Ca2+ channel function. J. Cell Biol. *169*, 435–445.

Seiler, K.P., George, G.A., Happ, M.P., Bodycombe, N.E., Carrinski, H.A., Norton, S., Brudz, S., Sullivan, J.P., Muhlich, J., Serrano, M., et al. (2008). ChemBank: a small-molecule screening and cheminformatics resource database. Nucleic Acids Res. *36*, D351–D359.

Shaw, P.J., and Feske, S. (2012). Physiological and pathophysiological functions of SOCE in the immune system. Front Biosci (Elite Ed) *4*, 2253–2268.

Shi, H., Liu, K., Xu, A., and Yao, S.Q. (2009). Small molecule microarray-facilitated screening of affinity-based probes (AfBPs) for gamma-secretase. Chem. Commun. (Camb.) *33*, 5030–5032.

Shi, H., Uttamchandani, M., and Yao, S.Q. (2011). Applying small molecule microarrays and resulting affinity probe cocktails for proteome profiling of mammalian cell lysates. Chem. Asian J. *6*, 2803–2815.

Takezawa, R., Cheng, H., Beck, A., Ishikawa, J., Launay, P., Kubota, H., Kinet, J.P., Fleig, A., Yamada, T., and Penner, R. (2006). A pyrazole derivative potently inhibits lymphocyte Ca2+ influx and cytokine production by facilitating transient receptor potential melastatin 4 channel activity. Mol. Pharmacol. *69*, 1413–1420.

Vegas, A.J., Fuller, J.H., and Koehler, A.N. (2008). Small-molecule microarrays as tools in ligand discovery. Chem. Soc. Rev. *37*, 1385–1394.

Vig, M., Peinelt, C., Beck, A., Koomoa, D.L., Rabah, D., Koblan-Huberson, M., Kraft, S., Turner, H., Fleig, A., Penner, R., and Kinet, J.P. (2006). CRACM1 is a plasma membrane protein essential for store-operated Ca2+ entry. Science *312*, 1220–1223.

Zhang, S.L., Yu, Y., Roos, J., Kozak, J.A., Deerinck, T.J., Ellisman, M.H., Stauderman, K.A., and Cahalan, M.D. (2005). STIM1 is a Ca2+ sensor that activates CRAC channels and migrates from the Ca2+ store to the plasma membrane. Nature *437*, 902–905.

